J Appl Physiol 118: 932–940, 2015.
First published January 29, 2015; doi:10.1152/japplphysiol.00902.2014.

Predicting the response of the injured lung to the mechanical breath profile

Bradford J. Smith,[1] Lennart K. A. Lundblad,[1] Michaela Kollisch-Singule,[2] Joshua Satalin,[2] Gary Nieman,[2] Nader Habashi,[3] and Jason H. T. Bates[1]

[1]*Vermont Lung Center, University of Vermont College of Medicine, Burlington, Vermont;* [2]*Department of Surgery, State University of New York Upstate Medical University, Syracuse, New York; and* [3]*R. Adams Cowley Shock Trauma Center, University of Maryland School of Medicine, Baltimore, Maryland*

Submitted 10 October 2014; accepted in final form 22 January 2015

Smith BJ, Lundblad LK, Kollisch-Singule M, Satalin J, Nieman G, Habashi N, Bates JH. Predicting the response of the injured lung to the mechanical breath profile. *J Appl Physiol* 118: 932–940, 2015. First published January 29, 2015; doi:10.1152/japplphysiol.00902.2014.—Mechanical ventilation is a crucial component of the supportive care provided to patients with acute respiratory distress syndrome. Current practice stipulates the use of a low tidal volume (V_T) of 6 ml/kg ideal body weight, the presumptive notion being that this limits overdistension of the tissues and thus reduces volutrauma. We have recently found, however, that airway pressure release ventilation (APRV) is efficacious at preventing ventilator-induced lung injury, yet APRV has a very different mechanical breath profile compared with conventional low-V_T ventilation. To gain insight into the relative merits of these two ventilation modes, we measured lung mechanics and derecruitability in rats before and following Tween lavage. We fit to these lung mechanics measurements a computational model of the lung that accounts for both the degree of tissue distension of the open lung and the amount of lung derecruitment that takes place as a function of time. Using this model, we predicted how tissue distension, open lung fraction, and intratidal recruitment vary as a function of ventilator settings both for conventional low-V_T ventilation and for APRV. Our predictions indicate that APRV is more effective at recruiting the lung than low-V_T ventilation, but without causing more overdistension of the tissues. On the other hand, low-V_T ventilation generally produces less intratidal recruitment than APRV. Predictions such as these may be useful for deciding on the relative benefits of different ventilation modes and thus may serve as a means for determining how to ventilate a given lung in the least injurious fashion.

ARDS; mechanical ventilation; predictive computational model; lung injury

MECHANICALLY VENTILATING PATIENTS with acute respiratory distress syndrome (ARDS) is a delicate balance between providing sufficient inspired volume with each breath to ensure adequate gas exchange, while at the same time avoiding ventilator induced lung injury (VILI). The damage resulting from VILI is a consequence of the repetitive stresses and strains that are applied to the lung tissues. These stresses and strains are reflected in the way that pressure, flow, and volume manifest at the airway opening throughout each breath, referred to collectively as the mechanical breath profile. Clearly, the mechanical breath profile contains important information about the potential for VILI to occur. Extracting this information, however, requires a quantitative understanding of how the mechanical breath profile translates into stress and strain at the tissue level, and then to tissue damage.

Address for reprint requests and other correspondence: J. H. T. Bates, 149 Beaumont Ave., HSRF 228, Burlington, VT 05405-0075 (e-mail: jason.h.bates@uvm.edu).

Presently, the link between the mechanical breath profile and VILI is understood only in general terms that are used to guide mechanical ventilation for the overall ARDS patient population. Thus, low tidal volumes (V_T) are used to reduce damage caused by tissue overdistension, known as volutrauma, with the goal for all ARDS patients being V_T = 6 ml/kg ideal body weight. Similarly, positive end-expiratory pressure (PEEP) is used to avoid the so-called atelectrauma that results from repetitive closure (derecruitment) and reopening (recruitment) of alveoli and small airways with each breath. It has been recognized for some time that the nature of the pressure-volume (PV) relationship of the lung may contain the information necessary to set the appropriate level of PEEP for a given patient (1, 14, 18, 32, 34, 48), but the precise manner in which PEEP should be set remains controversial (13, 17). Furthermore, almost all studies have neglected the important fact that recruitment and derecruitment are dynamic processes that depend on time as well as pressure (11). Finally, and perhaps most importantly, ventilation strategies that are efficacious for the ARDS patient population as a whole may be far from optimal in any given patient, especially given that ARDS is such a heterogeneous condition.

There is thus a critical need for predictive methods that can link a particular mechanical breath profile to VILI production in a given patient. Toward this end, we used a computational model to link measurements of airway pressure (Paw) and flow to tissue overdistension and repetitive recruitment in a rat model of ARDS. We then used the computational model to investigate how these two VILI mechanisms are modulated by the mechanical breath profile in two clinically established modes of mechanical ventilation.

METHODS

Animal preparation. All experiments were approved by the Animal Care and Use Committee of SUNY Upstate Medical University and conducted in accordance with National Institutes of Health guidelines. Ten male Sprague-Dawley rats (390–515 g) were anesthetized with 0.1 mg/kg ketamine and 0.011 mg/kg xylazine. A tracheostomy was performed, and a 2.5-mm cannula (Harvard Apparatus, Holliston, MA) was inserted and affixed to a Flexivent small-animal ventilator (SCIREQ, Montreal, QC, Canada). Baseline ventilation (V_T = 6 ml/kg, PEEP = 5 cmH_2O, 55 breaths/min) was applied for 5 min to allow the animals to stabilize. Lung injury was induced by instilling 2.5 ml/kg of 0.2% Tween 20 in normal saline into each lung, as previously described (27, 28). Following instillation, the rats were ventilated (V_T = 16 ml/kg, PEEP = 0) for 10 min to induce a modest degree of VILI, resulting in a reduction in alveolar size and increases in alveolar instability (27), conducting airway strain, and alveolar heterogeneity (28). The animals were not paralyzed, as is sometimes done to prevent spontaneous breathing activity from corrupting measurements of lung impedance, but there was no evidence of such

activity in the present study, and the model fits were all of good quality (see below).

Physiological measurements. All animals began the experiment in the healthy state from which they were subjected to the following protocol, all performed using the Flexivent ventilator. First, to standardize the lung volume (V_L) history, the lungs were recruited with a deep inspiration maneuver (DI) consisting of a 7-s pressure ramp from zero PEEP to a peak pressure of 30 cmH_2O followed by a 7-s hold at peak pressure. We then recorded a dynamic PV loop from zero PEEP at 1 Hz with a ventilator cylinder displacement = 9 ml to gather information about the nonlinear elastic properties of the open lung (see computational model analysis below). A second DI was performed to fully recruit the lung, and this was immediately followed by a derecruitability test, consisting of 5 min of ventilation with V_T = 6 ml/kg and PEEP = 0 that was interrupted at 20-s intervals, starting 6 s into the ventilation, by a 2-s multifrequency (0.5–20.5 Hz) volume perturbation (peak-peak ventilator cylinder displacement = 3 ml). The input impedance of the respiratory system was determined from each perturbation, and each impedance was fit with the constant-phase model (22), which provided a value for lung elastance (H). H increased progressively throughout each derecruitability test, which we took to reflect the propensity of the lungs to derecruit over time (3–5, 43, 44). Finally, another DI was performed to gather information about the recruitment characteristics of those lung units that had closed during the preceding derecruitability test.

After the induction of acute lung injury, a DI was first applied to standardize V_L history, followed by the recording of a dynamic PV loop at PEEP = 0. We then recorded four measurement sequences, each consisting of a DI followed by a derecruitability test and then a second DI. These sequences were separated by a 20-s period of 6 ml/kg ventilation. The four derecruitability tests were performed sequentially at PEEP levels of 0, 3, 6, and 12 cmH_2O with the DIs applied above the prescribed PEEP to reach a maximum of 30 cmH_2O.

Computational model. The experimental data were analyzed with the aid of a computational model adapted from our previously reported studies (11, 31, 46, 47). The model is composed of N_{Units} = 768 parallel respiratory units (RU), each connected to a common airway junction. (This number of units was selected to provide a smooth response during recruitment and derecruitment while maintaining reasonable program execution times.) Each RU consists of a terminal airway connecting to an alveolar compartment. Each alveolar compartment has an identical nonlinear elastance unit (E_{Unit}) given by

$$E_{Unit}(V_{Unit}) = N_{Units}\begin{cases} E_{Base}, & \text{if } V_{Unit} \le V_{Crit}/N_{Units} \\ E_{Base} + E_{Fac}\{N_{Units}[V_{Unit} - (V_{Crit}/N_{Units})]\}^2, & \text{if } V_{Unit} > V_{Crit}/N_{Units} \end{cases} \quad (1)$$

where V_{Unit} is the compartment volume, V_{Crit} is the volume at which E_{Unit} transitions from linear to nonlinear (volume dependent) behavior, $1.1 \le E_{Base} \le 1.4$ cmH_2O/ml is the low-volume (linear) elastance equivalent to the value of H measured in the healthy animal, and E_{Fac} is the rate constant for the volume-dependent elastance increase in the nonlinear regime. The values of the parameters V_{Crit}, E_{Unit}, and E_{Fac} were determined by fitting the model to experimental data (see below). The elastance of the entire model (E_L) thus changes with the number of open units according to

$$E_L(t) = \left[\sum \text{open units}\left(\frac{1}{E^i_{Unit}(V^i_{Unit})}\right)\right]^{-1} \quad (2)$$

Likewise, the airflow resistance for the entire model (R_{mod}) is

$$R_{mod}(t) = R_{unit}[N_{open}(t)]^{-1} \quad (3)$$

with $R_{Unit} = N_{Units}$·Raw. The airway resistance (Raw) $0.02 \le$ Raw ≤ 0.05 $cmH_2O{\cdot}s{\cdot}ml^{-1}$ was experimentally determined for each rat by equating it to the Newtonian resistance parameter of the constant phase model that was fit to each respiratory impedance measurement (22). The magnitude of the airflow ($\dot{Q}$), therefore, depended on the pressure differential between the lung (P_L) and ventilator (P_{vent}) in the manner first described by Rohrer (39) so that the magnitude of the tracheal flow rate was

$$|\dot{Q}| = \frac{R_1 - \sqrt{R_1^2 + 4R_2|P_L - P_{vent}|}}{2R_2} \quad (4)$$

with $R_2 = 0.003$ selected to match the peak expiratory flow (PEF) rates measured in Sprague-Dawley rats by Wright et al. (53). The constant $R_1 = R_{eq} + R_{mod}$ and the resistance of the ventilator tubing (R_{eq}) was measured during the ventilator calibration procedure for each rat so that $0.06 \le R_{eq} \le 0.1$ $cmH_2O{\cdot}s{\cdot}ml^{-1}$.

$|\dot{Q}|$ is used to calculate the Paw = $P_L + dR_1|\dot{Q}|$, with $d = 1$ when $P_L \ge P_{vent}$, and $d = -1$ when $P_L < P_{vent}$. The flow into each open RU is then $(Paw - E_{Unit}V_{Unit})/R_{Unit}$. The V_L is defined as the sum of the volumes of all open RUs so that $P_L = E_L V_L$. This formulation allows for gas to be trapped when an RU derecruits, such that the volume of the closed unit is not counted toward the total V_L.

When simulating pressure-controlled ventilation, the model was driven with a prescribed pressure waveform. For volume-controlled ventilation, the model was driven with a prescribed volume waveform operating on a shunt gas elastance (E_{gas}) of $14 < E_{gas} < 27$ cmH_2O/ml, representing the compressibility of the air in the Flexivent cylinder. E_{gas} was determined during the equipment calibration procedure performed before each experiment (43).

To simulate a derecruitability test, it is necessary to take the dynamics of recruitment and derecruitment into account. This is achieved using virtual trajectories, as our laboratory has previously described (11, 30, 31, 47), that provide an empirical representation of the way in which recruitment and derecruitment of lung units depend on both pressure and time. In brief, each RU is associated with a virtual trajectory variable $0 \le x \le 1$ that increases at a rate S_O (P_O − Paw) when Paw is greater than a critical opening pressure (P_O), where S_O is the opening velocity constant. Conversely, when Paw is less than the critical closing pressure P_C, then x decreases at a rate given by the closing velocity constant (S_C). The recruitment and derecruitment dynamics of the model are governed by the probability distribution functions from which P_C, P_O, S_C, and S_O are randomly drawn.

Based on a previous study in mice with VILI (47), we employed two groups of RU having different distributions for P_C, P_O, S_C, and S_O. One group contained $(1 - \beta)N_{Units}$ units, with S_C and S_O drawn from exponential probability density functions given by $f(x) = e^{x/\lambda_c}/\lambda_c$ and $f(x) = e^{x/\lambda_o}/\lambda_o$, respectively, where $\lambda_O = 0.1\lambda_C$ (31). λc and λ_o are the scale parameters for the distribution of closing and opening velocities, respectively, and β defines the fraction of the lung in each group of respiratory units that exhibits similar recruitment characteristics. P_C was drawn from a Gaussian distribution having mean μ_C and SD σ_C (11, 12, 23, 38, 47), while $P_O = P_C + \Delta P$. The parameters λ_C, μ_C, σ_C, and change in pressure (ΔP) were determined for each rat during the model fitting process (see below).

The other population of βN_{Units} RU had $\lambda_C = 0.075$ and $\lambda_O = 0.75$, with P_C drawn from a uniform probability density function on the interval (16, 30) to match the long-timescale closure observed in the derecruitment tests and the rapid reopening during DIs. To accommodate recruitment, which was observed during the 14-s DIs and not during 55 breaths/min ventilation, we set $P_O = P_C$ and define a latency time parameter for each RU (T_S), which is drawn from a Gaussian distribution with a mean $\mu_T = 0.45$ s and SD $\sigma_T = 0.05$ s. When Paw < P_C, the virtual trajectory decreases at a rate $dx{\cdot}dt^{-1} = S_C$, as described above. However, Paw must remain above P_O for a period T_S before the virtual trajectory is allowed to increase at a rate $dx/dt = S_O$ (P_O − Paw). The model equations were integrated using the forward Euler method at a simulation frequency of 500 Hz.

Model fitting. The free model parameters that were evaluated during the model-fitting procedure are listed in Table 1. The model was fit to the experimental data from each rat both before and after Tween instillation using a parallel pattern search (PPS) optimization

Table 1. *Initial value, lower and upper bounds, and the initial grid step size for the parameters determined using the numerical optimization algorithm*

Parameter	Starting Value	Minimum	Maximum	Initial Grid Step Size
E_{Fac}, cmH_2O/ml^3	0.04	0.01	0.2	0.015
V_{Crit}, ml	8	4	12	1.5
ΔP, cmH_2O	6	0	18	2
μ_C, cmH_2O	5	−1	14	2.5
σ_C, cmH_2O	3	0.5	9	2.5
λ_C, s/cmH_2O	50	0.01	100	12.5
β	0.2	0	0.8	0.15

See text for definition of terms.

algorithm (24–26, 29, 50) as our laboratory has described previously (46). Briefly, this algorithm seeks to minimize an objective function quantifying the differences between the predicted and measured pressures, volumes, and elastances. At each iteration of the PPS algorithm, this objective function is examined for every one of the 2,187 distinct combinations of the 7 parameters listed in Table 1. The seven-dimensional parameter grid is composed of the current parameter estimates as well the current values, both plus and minus the current grid step size. If the value of the objective function at any of these points is less than its current minimum value, then the center of the multidimensional search grid is relocated to the position of the new minimum. Otherwise, the grid spacing is reduced by 40% for the next iteration. The search for the global minimum of the objective function is terminated when the grid step size has been reduced 10-fold or after 30 iterations.

For each animal, under either baseline conditions or postinjury, the computational model was fit to all physiological data simultaneously by minimizing the composite cost function

$$Y = E_{DI} \cdot \left(nt_{DI} \cdot N_{DI}\right)^{-1} + E_{PV} \cdot \left(nt_{PV} \cdot N_{PV}\right)^{-1} + 5E_{DTest} \cdot N_{DTest}{}^{-1} \quad (5)$$

where E_{DTest} is the root mean square (RMS) error between the measured and calculated elastance values at each simulation point during the derecruitability tests. E_{PV} is the RMS pressure error during the volume-controlled dynamic PV loops, and E_{DI} is the RMS error in the delivered volume during the pressure-controlled DI maneuvers. N_{DI}, N_{PV}, and N_{DTest} are the numbers of DI maneuvers, dynamic PV loops, and the derecruitability test elastance measurements, respectively, that were performed in a given rat. For the healthy rats N_{DI} = 2, N_{PV} = 1, and N_{DTest} = 13, while for the injured rats N_{DI} = 8, N_{PV} = 1, and N_{DTest} = 52. The number of time points in each DI maneuver nt_{DI} = 6,000, and the number of time points in each PV loop nt_{PV} = 525.

To reduce the computational cost of the simulations, we retain the computed values of Y (*Eq. 5*) at each step. If an identical parameter combination is used in a subsequent PPS step, the retained Y is used to avoid reevaluating the model. For each animal and treatment condition (healthy or injured), we use a constant value to seed the random number generator that generates the distributions of P_C and S_C throughout the PPS model evaluations and model simulations (described below). This approach improves convergence of the PPS algorithm because Y computed for a given set of parameters remains constant, removing a small amount of random noise from the error surface. Fifty iterations of the model using the best-fit parameters with the random number generator seed based on the wall clock time provided a coefficient of variation in Y of 0.044 for the healthy simulations and 0.13 for the injured cases. The mean of the SD in open fraction at each time point was 0.012 for both the healthy and injured rats.

Model simulations. Once the model was fit to each of the rats, we assessed the potential for producing volutrauma and atelectrauma during mechanical ventilation under both baseline and postinjury conditions. We first performed this investigation for the low-V_T ventilation (LTVV) that is now standard of care for ARDS patients, but which was adapted here to be appropriate for the rat. The LTVV had an inspiratory-to-expiratory duration ratio of 1 to 1.5, a rate of 55 breaths/min, and a V_T of 6 ml/kg, achieved by applying an inspiratory pressure (P_I) ramp beginning at the applied level of PEEP and increasing for 0.05 s at the rate necessary to achieve the desired V_T. The P_I was determined by iteratively performing recruitment maneuvers and ventilating until the lung open fraction stabilized to achieved the desired V_T = 6 ml/kg. Expiration was passive against the prescribed PEEP after ramping down for 0.05 s from the peak P_I.

We also simulated airway pressure release ventilation (APRV) which consists of periods of sustained P_I of inspiratory time duration, interrupted periodically by brief expiratory phases of duration designed to achieve a desired end-expiratory flow (EEF) as a percentage of PEF. An EEF-to-PEF ratio (EEF/PEF) of 75% is well established as the appropriate clinical setting for APRV (21, 27). We investigated EEF/PEF ranging from 75% (corresponding to a relatively short expiratory duration) to 10% (corresponding to a longer expiratory duration). In a second series of simulations, we investigated the effects of $5 \leq P_I \leq 50$ cmH_2O for an EEF/PEF of 75%. In each case, inspiratory time was iteratively adjusted to achieve a minute ventilation of 330 $ml \cdot kg^{-1} \cdot min^{-1}$, which was identical to that delivered with LTVV (measured at steady state following a DI). The expiratory pressure (P_E) was 0 cmH_2O in all cases with a ramp of 0.05 s between P_I and P_E to represent the noninstantaneous transition between these two pressures that is observed experimentally (27, 28). Because of the high expiratory flows occurring early in expiration in APRV, we increased the simulation frequency to 2,000 Hz for all model simulations to improve the accuracy of our calculations.

RESULTS

Figure 1 shows data and model fits obtained in a representative rat. When the animal was healthy, its compliance decreased above the predicted V_{Crit} = 8.6 ml, presumably due to strain stiffening of the lung tissues at high volumes (Fig. 1*A*). In contrast, after the rat was injured, the slope of the PV curve increased for Paw > 15 cmH_2O, indicative of ongoing recruitment. The model calculated that the open fraction of the lung in the injured animal increased from 0.28 to 0.96 between Paw = 15 cmH_2O and 30 cmH_2O. Figure 1*B* shows the dynamic PV loop for the same animal, after injury, illustrating the marked hysteresis that resulted from the inspiratory recruitment of closed lung units that reclosed during the subsequent expiration. Figure 1*C* shows the corresponding time courses of H during each derecruitability test, again after the animal was injured.

Figure 2 shows the derecruitability test data and model fits for seven of the rats we studied. Two of the 10 animals in the experiment were excluded due to incomplete data, and a third animal was excluded because the baseline H measurements were more than 5 SDs above the mean of the remaining 7 animals. These three animals were also excluded from all subsequent analyses. The data in Fig. 2 are similar to those of the single rat shown in Fig. 1*C* and show that H increased progressively with time during each of the individual derecruitability tests, reflecting progressive closure of lung units (2, 6). There were dramatic increases in both the magnitude and rate of change of H at PEEP = 0 cmH_2O in the injured rats compared with the healthy animals, indicating a correspondingly increased magnitude and rate of derecruitment. The fits of the computational model to these data provide estimates of the mean open fraction to be 0.67 for the healthy animals with

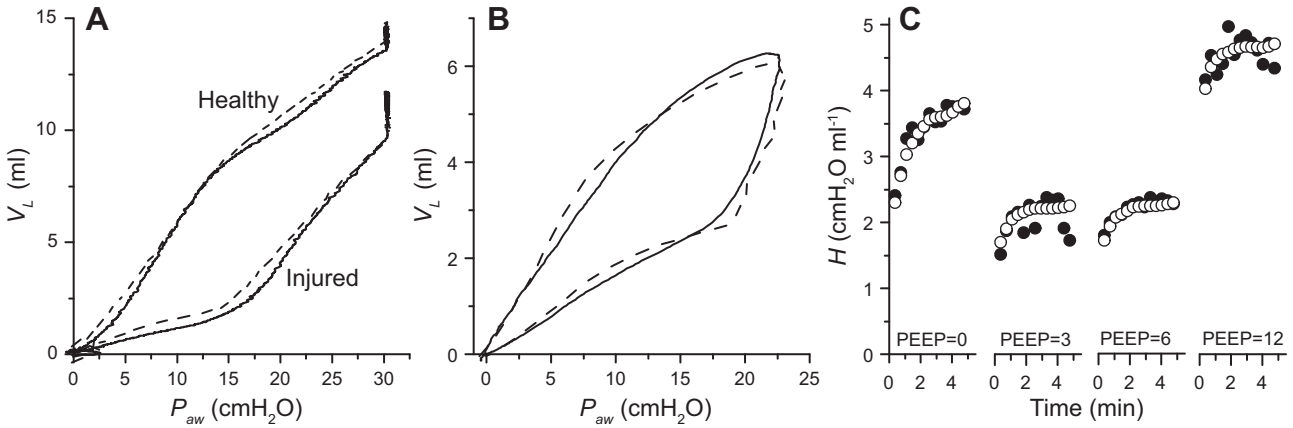

Fig. 1. Data from a representative rat. *A*: measured (solid lines) and modeled (dashed lines) relationships between airway pressure (Paw) and lung volume above functional residual capacity (V_L) obtained during a deep inspiration recruitment maneuver in the healthy state and after lung injury was induced by Tween lavage. *B*: measured (solid line) and modeled (dashed line) dynamic pressure-volume loops in the injured animal. *C*: measured (●) and modeled (○) elastance (H) during derecruitability tests in the injured animal performed at positive end-expiratory pressure (PEEP) levels of 0, 3, 6, and 12 cmH_2O.

PEEP = 0 cmH_2O. Following injury, the mean open fraction estimates are 0.33, 0.51, 0.66, and 0.80 for PEEP = 0, 3, 6, and 12 cmH_2O, respectively.

The increased derecruitability of the injured lung is reflected in the best-fit model parameter values (Table 2). A significant difference was found between the healthy and injured rats for λ_C, indicating that derecruitment and recruitment both occurred more rapidly in the injured animals. Furthermore, since ΔP was also significantly increased, the reopening occurred at higher pressures in the injured animals. Finally, the transition to nonlinear elastance occurred at a lower V_L, V_{crit}, in the injured animals (Table 2).

Figure 3*A* shows model predictions of lung distension for both healthy (black) and injured (red) rats during LTVV over a range of PEEP levels from 0 to 25 cmH_2O. The degree of lung distension is a measure of the extent to which the lung tissues are stretched and is defined here as the ratio of the lung's volume to its open fraction (i.e., distension increases as a given volume is accommodated by a decreasing fraction of the total lung tissue). Figure 3 shows both the maximum value of lung distension achieved at the end of inspiration and the minimum value achieved at the end of expiration. Also shown is the lung distension at which the PV behavior of the lung tissue transitions from linear to nonlinear in the healthy rats (black dotted line). Interestingly, this transition occurs at a lower distension in the injured rats (red dotted line) than in the healthy animals, because injury changed the apparent properties of the tissue so that they became nonlinear at lower volumes (Table 2), likely as a result of alveolar collapse due to surfactant inactivation and air displaced by the instilled Tween. Figure 3*B* shows corresponding plots for the rats ventilated with APRV, with EEF/PEF ranging from 10 to 75%, corresponding to progressively decreasing expiratory durations.

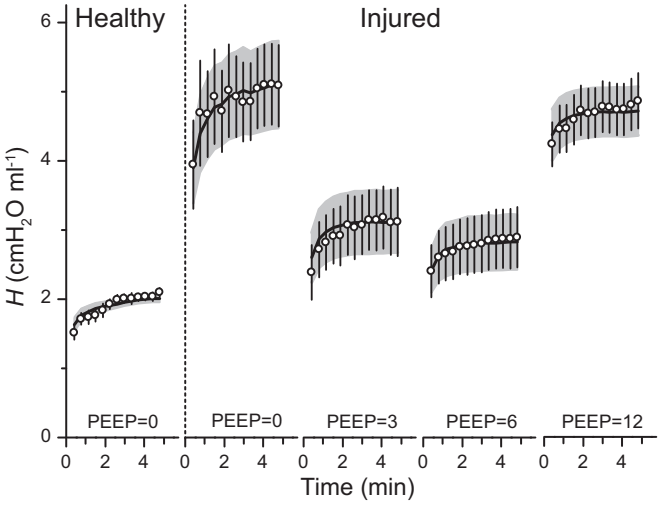

Fig. 2. Mean (±SE) H measured during derecruitability tests performed at different PEEP levels in 7 rats (○), together with the mean of the model fits (solid curves, gray shading is ±SE).

The maximum and minimum values of open fraction predicted by the computational model for both healthy and injured rats are shown for LTVV and APRV in Fig. 4, *A* and *B*, respectively. LTVV always avoids significant intratidal recruitment (Fig. 4*A*), but at the expense of incomplete recruitment, as PEEP decreases below its maximum value of 25 cmH_2O. In contrast, APRV always achieves full recruitment at end inspiration due to the high prescribed P_I, but, as the EEF decreases (i.e., longer expiratory durations), the degree of intratidal derecruitment increases (Fig. 4*B*). What is particularly striking about these predictions is that, while intratidal recruitment is always rather small in healthy animals (Fig. 4*B*, black), longer durations of the expiratory phase in the injured rats can result

Table 2. *Best fit parameters for healthy and lung-injured rats*

Parameter	Healthy Rats	Injured Rats
E_{Fac}, cmH_2O/ml^3	0.048 ± 0.012	0.047 ± 0.010
V_{Crit}, ml	9.22 ± 0.78	5.81 ± 0.49*
ΔP, cmH_2O	3.62 ± 1.29	12.77 ± 1.96*
μ_C, cmH_2O	0.77 ± 0.13	2.65 ± 0.79
σ_C, cmH_2O	2.15 ± 0.96	5.61 ± 0.59
λ_C, s/cmH_2O	8.83 ± 2.84	54.28 ± 12.64*
β	0.15 ± 0.055	0.08 ± 0.026

Values are means ± SE. *Significant difference between the parameter values following lung injury identified with paired *t*-tests (α = 0.05).

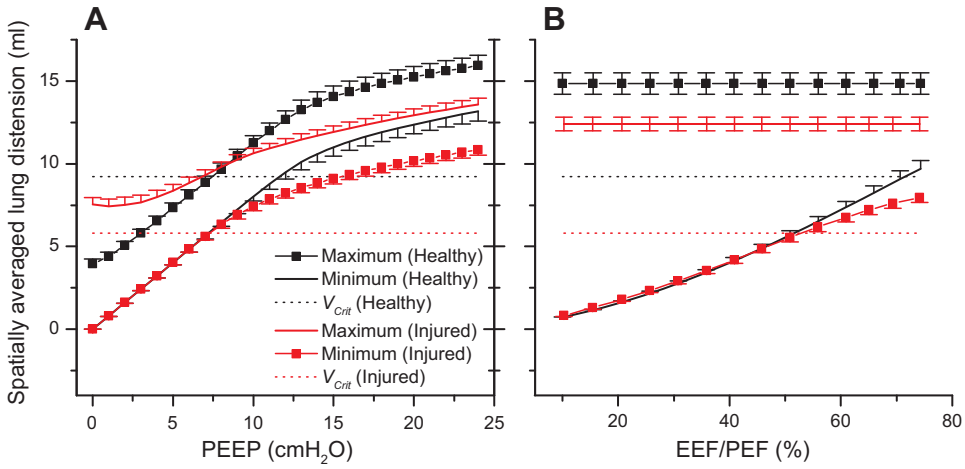

Fig. 3. Minimum and maximum of the spatially averaged distension of the open lung tissue (corresponding to end-expiration and end-inspiration, respectively) during low-tidal volume ventilation (LTVV; *A*) and airway pressure release ventilation (APRV) at inspiratory pressure (P_I) = 36 cmH_2O (*B*) predicted from the model fits to 7 rats (means ± SE) in healthy animals (black) and after induction of lung injury (red). Also shown (dotted lines) are the threshold volumes at which the lung pressure-volume relationship becomes nonlinear (V_{Crit}). EEF/PEF, ratio of end-expiratory flow to peak expiratory flow.

in nearly one-half the lung closing and reopening with each breath (Fig. 4*B*, red), highlighting the clinical importance of using APRV with its proper setting of EEF/PEF = 75%. Both modes of ventilation converge on the same recruitment characteristics either as PEEP increases in LTVV (Fig. 4*A*), or as expiratory duration shortens in APRV (Fig. 4*B*).

In Fig. 5, we compare the recruitment and spatially averaged open lung distension characteristics of LTVV as a function of PEEP, as well those of APRV over a range of P_I with EEF/PEF = 75%. For a given peak P_I, both modes of ventilation produce similar levels of spatially averaged distension of the open lung, but the excursions in distension with APRV are lower than those of LTVV at low PEEP and higher at high PEEP (Fig. 5*A*). There are also differences in recruitment between the two modes of ventilation (Fig. 5*B*), the most noticeable being that LTVV produces substantially less open lung at low pressures compared with APRV. At the high P_I typically used clinically (>25 cmH_2O), APRV again maintains more open lung, but only by ~6%, which may not be clinically significant.

DISCUSSION

The ARDSnet clinical trials (9) demonstrated improved outcomes in ARDS patients ventilated with a V_T of 6 ml/kg ideal body weight, which may be decreased to 4 ml/kg to prevent plateau pressures from exceeding 30 cmH_2O. The clinical protocol also stipulated that PEEP and inspired O_2 fraction should be set to achieve 55 ≤ arterial P_{O_2} ≤ 80 Torr, and that respiratory rate should be adjusted to balance pH. These criteria are based on empirical findings and are not linked directly to the underlying mechanisms that cause VILI, even though they are rationalized by the notion of ventilating the "baby lung" and thus of reducing volutrauma by limiting the injurious effects of over-stretching the healthier lung regions (9). Also, despite the documented survival benefit of the ARDSnet trial, there has been little additional evidence that LTVV coupled with control of other factors, such as PEEP, mean Paw, or ventilator mode, correlates with a reduction in volutrauma as a marker of overdistension (8, 9, 15, 33, 35, 42, 49, 54).

A limitation of the ARDSnet ventilation protocol is the universal application to all ARDS patients, despite the fact that this patient population is highly heterogeneous. The shortcomings of this approach, and the efficacy of personalized ventilation determined via respiratory mechanics, is highlighted in a recent clinical investigation involving H1N1 influenza patients diagnosed with ARDS and refractory hypoxemia and referred for extracorporeal membrane oxygenation (20). In that study, respiratory system elastance was partitioned into lung and

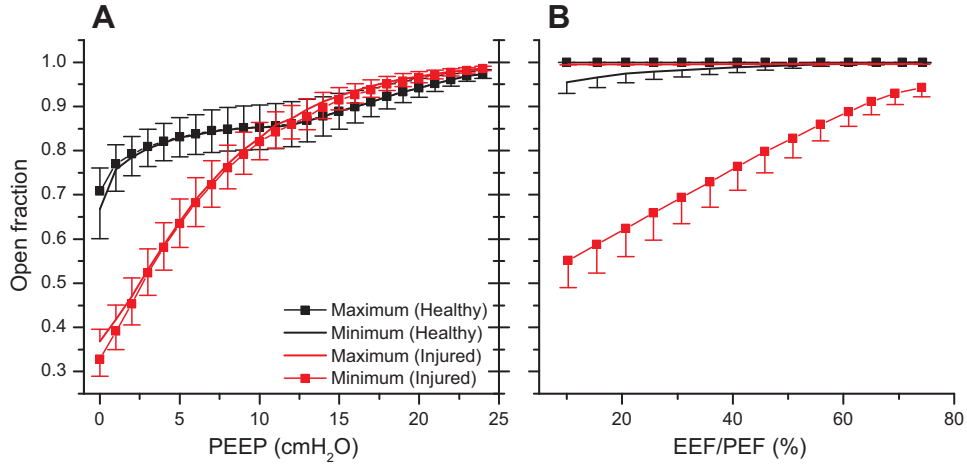

Fig. 4. Minimum and maximum open lung fraction during LTVV (*A*) and APRV at P_I = 36 cmH_2O (*B*) predicted from the model fits to 7 rats (mean ± SE) in healthy animals (black) and after induction of lung injury (red).

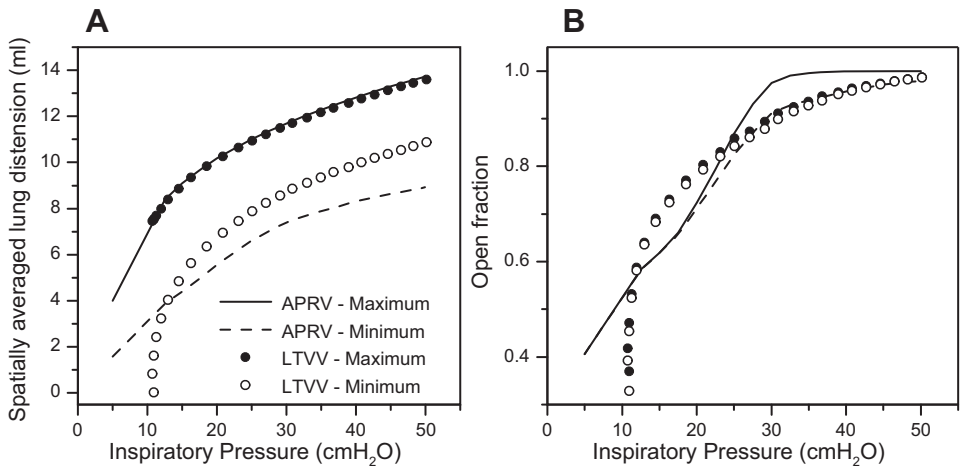

Fig. 5. Predicted spatially averaged lung tissue distension (*A*) and open lung fraction (*B*) in lung-injured rats. The maximum and minimum values for APRV with a EEF/PEF of 75% and $5 \leq P_I \leq 50$ cmH_2O are shown with solid and dashed lines, respectively. Also shown are the maximum (●) and minimum (○) for LTVV with $0 \leq PEEP \leq 24$ cmH_2O.

chest wall components, and PEEP was titrated to achieve a transpulmonary pressure of ~25 cmH_2O. In subjects with abnormally high chest wall elastance, this lead to PEEP ≈ 22 cmH_2O and plateau pressures approaching 40 cmH_2O. These high ventilation pressures resolved the refractory hypoxemia and the need for extracorporeal membrane oxygenation rescue in all of the patients in this subgroup.

Furthermore, the measures described in the ARDSnet protocol are only implemented once ARDS has developed and thus represent a reactionary measure rather than a proactive strategy. It is thus reasonable to suppose that improved approaches to ventilating the injured lung would avoid these limitations by basing decisions on the assessment of the two key mechanisms believed to contribute to VILI, namely overdistension of parenchymal tissues and repetitive recruitment of closed lung units, and by preemptive avoidance of the progressive functional degradation associated with clinical ARDS (45). However, tissue overdistension and repetitive recruitment cannot be monitored directly in the lungs of an ARDS patient. Instead, these injurious processes must be inferred from measureable quantities in which they are reflected. Fortunately, pressure and flow at the airway opening are perfect candidates in both regards. Nevertheless, patterns of overdistension and recruitment can only be extracted from Paw and airway flow via the intermediary of a computational model of lung mechanical function. On the basis of our laboratory's previous studies (10, 44, 46, 47), we identified a suitable model for this purpose and found that it can accurately recapitulate the mechanical behavior of the injured lung during a variety of different maneuvers that collectively reveal its dynamic and nonlinear behavior (Figs. 1 and 2).

To the extent that the mechanisms represented in our computational model correspond to those present in a real lung, we are then able to make predictions about the injurious processes occurring within a given lung during a prescribed regimen of mechanical ventilation. In the present study, we focus on two particular ventilation modes. The LTVV mode now widely serves as a standard of care due to the success of the ARDSnet trial (9). APRV is often considered a rescue mode for patients with established ARDS rather than a primary mode of ventilation (7, 16, 21), but it has been investigated as a primary mode and has been shown with early application to significantly reduce ARDS incidence and mortality (7). In the present study, we made predictions concerning these two modes of ventilation in rats because the model was fitted to data measured in rats, but there is no reason in principle why the same approach could not be used in human patients once the necessary dynamic lung function data are in hand.

First, we compared the degree of tissue distension occurring with LTVV vs. APRV (Fig. 3) and identified some immediately obvious differences. Most importantly, while distension is roughly proportional to PEEP with LTVV and does not achieve high levels until PEEP is correspondingly high (Fig. 3*A*), distension is always relatively high with APRV (Fig. 3*B*) because we maintain $P_I = 36$ cmH_2O. At corresponding plateau pressures, LTVV and APRV demonstrate an equivalent level of spatially averaged distension as shown in Fig. 5. Furthermore, the excursion in tissue distension during a breath (i.e., from end-expiration to end-inspiration) is relatively unaffected by PEEP in LTVV because of the fixed V_T. In contrast, the range of tissue distension is highly dependent on the duration of the expiratory phase in APRV, where V_T is dependent on the targeted EEF/PEF, and this applies to both normal and injured lungs. For example EEF/PEF of 75 and 10%, respectively, provide average V_T values of 10.7 and 26.5 ml/kg in the injured animals for $P_I = 36$ cmH_2O. However, when the EEF/PEF is held at 75%, the distension range remains roughly constant at higher values of P_I, but is decreased at low P_I due to the reduced V_T values (Fig. 5*A*). LTVV and APRV also differ somewhat in their recruitment characteristics (Fig. 5*B*), although these differences are not particularly large, except perhaps at low minimum pressures where LTVV allow for substantially more derecruitment than APRV (Fig. 5*B*).

On the other hand, APRV with an extended duration of $P_I = 36$ cmH_2O is generally better than LTVV at keeping the lungs recruited, as shown in Fig. 4, *B* and *A*, respectively. Because of both the pressure and time dependence of recruitment, APRV in the healthy lung maintains full recruitment during the plateau phase with very little derecruitment at all levels of EEF (Fig. 4*B*). Inspiratory recruitment also remains complete in the injured lung, but derecruitment during expiration increases rapidly with increasing expiratory duration. This demonstrates why it is so important to use APRV with the proper setting of EEF/PEF = 75%; when EEF/PEF is set improperly at 10%, the model predicts a substantial amount of intratidal recruitment

and derecruitment that could be very damaging to the lung tissues. In contrast, LTVV predicts minimal intratidal recruitment and derecruitment, but at the expense of a substantial residual level of derecruitment at end-inspiration until PEEP reaches at least 15 cmH_2O (Fig. 4*A*). Since there is no benefit to longer expiratory times with APRV, we simulated the effects of varied P_I with the PEF/EEF fixed at 75%, consistent with previously published guidelines (21). To facilitate direct comparison with the LTVV simulations, we plot the predicted spatially averaged distension and open fraction for the injured rats against the prescribed P_I in Fig. 5, which shows that maximum of the mean open lung distension is directly related to P_I, regardless of the mode of ventilation. For $P_I > 25$ cmH_2O, where such injured lung would likely be ventilated clinically, our predictions indicate that, for a given level of distension, APRV provides greater recruitment than LTVV, but without increasing overdistension.

These predictions thus show that LTVV and APRV have complementary strengths and weaknesses, which are strongly dependent on the functional state of the lung and the applied mechanical breath profile. When directly comparing the two modes at comparable levels of maximum tissue distension in the injured lung (Fig. 5), we predict APRV will improve recruitment in the range of P_I values that would be applied to the injured lung. However, the range of distension and open fraction are less with LTVV. Precisely how these various factors translate into clinical outcomes remains to be determined, because we do not yet have a way of equating the rate of generation of VILI to some function of overdistension, intratidal recruitment and distension, and maximum amount of open lung. Nevertheless, the modeling methodology we have employed here establishes a basis on which an injury cost function for VILI might be developed. This supposition, however, must be viewed relative to a number of important limitations of our study.

Perhaps the most important limitation is the fact that we have based our analysis of the relative merits of LTVV and APRV on a computational model that contains a number of critical assumptions. We assume, for example, that overdistension applies equally to all regions of open lung because we assume that these regions all experience essentially the same distending pressure due to homogeneous resistance, and that each alveoli has an identical stress-strain relationship (e.g., equal V_{Crit} and E_{Base}). There are numerous factors that this ignores, including gravity-dependent differences in pleural pressure that play an important role in clinical ARDS and variations in the local stress-strain behavior of the parenchyma resulting from ventilation inhomogeneity. In addition, our model predictions are representative of a passively ventilated patient and, therefore, do not account for the effects of spontaneous breathing, which has been shown during APRV to improve recruitment (52), end-expiratory V_L (51), and ventilation of the dependent lung (36). Thus there may be additional benefits to APRV in patients exhibiting spontaneous inspiratory efforts that are not included in our predictions. Trying to account for these effects would greatly complicate the model and model fitting, and it is unclear that the gains would be worth the effort. Perhaps even more critical is our assumption of a mechanism for the time dependence of recruitment and derecruitment based on the use of virtual trajectories (10, 31). The behavior of these virtual trajectories bears distinct resemblance to processes involved in airway collapse and reopening that have been studied extensively in the laboratory (19, 37), which perhaps lends some credibility to their use in the present application. Nevertheless, they remain an essentially empirical mechanism.

Another potential and important limitation of our study concerns is translatability to the human patient. For example, we have neglected gravitational gradients in the present study, because these are essentially unimportant in the small lung of the rat, but they are significant in a human lung. Also, finding model parameter values that accurately embody recruitment and derecruitment dynamics requires perturbing the lung experimentally under a rather wide amplitude range of pressure, flow, and volume (Figs. 1 and 2). It remains to be seen whether it is possible to safely obtain a rich enough data set for this purpose in human patients, particularly those with injured lungs. One promising approach might be to use Paw and airway flow data collected during variable V_T ventilation, a new approach to mechanical ventilation that has been shown to have certain physiological advantages over conventional ventilation and that we have recently shown allows the dynamics of recruitment and derecruitment to be identified (46).

In summary, we have shown in rats that measuring Paw and airway flows during a sufficiently rich set of dynamic perturbations allows the identification of a computational model embodying the injurious mechanisms of both tissue overdistension and repetitive recruitment. We then used the model to simulate lung distension and recruitment during LTVV with a range of PEEP levels and during APRV with a range of expiratory durations and P_I values. These simulations indicate that LTVV produces somewhat less intratidal recruitment than APRV. However, when APRV is properly set with EEF/PEF = 75% at clinically relevant pressures in the injured lung, it achieves a higher level of open lung than LTVV and does not result in additional tissue distension. Our model thus demonstrates that both the timing and magnitude of the pressures applied during mechanical ventilation play a role in recruitment, while the spatially averaged maximum tissue distension is a function of P_I. Taken together with our porcine model of ARDS, which exhibited improved oxygenation and lung compliance when ventilated with APRV compared with LTVV (40, 41), and a recent meta-analysis that suggests that properly set APRV appears to reduce ARDS incidence and in-hospital mortality (7), our simulations suggest that the protective benefits of recruitment may outweigh the damage caused by tissue overdistension.

GRANTS

This work was supported by National Institutes of Health Grants P30 GM-103532, T32 HL-076122, R01 HL-124052, and R21 HL-092801. High-performance computing resources were provided by the Vermont Advanced Computing Core at the University of Vermont supported by National Aeronautics and Space Administration Grant NNX-06AC88G.

DISCLOSURES

No conflicts of interest, financial or otherwise, are declared by the author(s).

AUTHOR CONTRIBUTIONS

Author contributions: B.J.S., G.F.N., N.H., and J.H.B. conception and design of research; B.J.S., L.K.L., M.K.-S., J.S., and G.F.N. performed experiments; B.J.S. and G.F.N. analyzed data; B.J.S., L.K.L., M.K.-S., J.S., G.F.N., N.H., and J.H.B. interpreted results of experiments; B.J.S. and J.H.B.

prepared figures; B.J.S. drafted manuscript; B.J.S., L.K.L., M.K.-S., J.S., G.F.N., N.H., and J.H.B. edited and revised manuscript; B.J.S., L.K.L., M.K.-S., J.S., G.F.N., N.H., and J.H.B. approved final version of manuscript.

REFERENCES

1. **Albaiceta GM, Taboada F, Parra D, Luyando LH, Calvo J, Menendez R, Otero J.** Tomographic study of the inflection points of the pressure-volume curve in acute lung injury. *Am J Respir Crit Care Med* 170: 1066–1072, 2004.
2. **Albert SP, DiRocco J, Allen GB, Bates JHT, Lafollette R, Kubiak BD, Fischer J, Maroney S, Nieman GF.** The role of time and pressure on alveolar recruitment. *J Appl Physiol* 106: 757–765, 2009.
3. **Allen G, Bates JH.** Dynamic mechanical consequences of deep inflation in mice depend on type and degree of lung injury. *J Appl Physiol* 96: 293–300, 2004.
4. **Allen G, Lundblad LK, Parsons P, Bates JH.** Transient mechanical benefits of a deep inflation in the injured mouse lung. *J Appl Physiol* 93: 1709–1715, 2002.
5. **Allen GB, Leclair T, Cloutier M, Thompson-Figueroa J, Bates JH.** The response to recruitment worsens with progression of lung injury and fibrin accumulation in a mouse model of acid aspiration. *Am J Physiol Lung Cell Mol Physiol* 292: L1580–L1589, 2007.
6. **Allen GB, Pavone LA, DiRocco JD, Bates JH, Nieman GF.** Pulmonary impedance and alveolar instability during injurious ventilation in rats. *J Appl Physiol* 99: 723–730, 2005.
7. **Andrews PL, Shiber JR, Jaruga-Killeen E, Roy S, Sadowitz B, O'Toole RV, Gatto LA, Nieman GF, Scalea T, Habashi NM.** Early application of airway pressure release ventilation may reduce mortality in high-risk trauma patients: a systematic review of observational trauma ARDS literature. *J Trauma Acute Care Surg* 75: 635–641, 2013.
8. **Anzueto A, Frutos-Vivar F, Esteban A, Alia I, Brochard L, Stewart T, Benito S, Tobin MJ, Elizalde J, Palizas F, David CM, Pimentel J, Gonzalez M, Soto L, D'Empaire G, Pelosi P.** Incidence, risk factors and outcome of barotrauma in mechanically ventilated patients. *Intensive Care Med* 30: 612–619, 2004.
9. **ARDSnet.** Ventilation with lower tidal volumes as compared with traditional tidal volumes for acute lung injury and the acute respiratory distress syndrome. The Acute Respiratory Distress Syndrome Network. *N Engl J Med* 342: 1301–1308, 2000.
10. **Bates JH, Irvin CG.** Time dependence of recruitment and derecruitment in the lung: a theoretical model. *J Appl Physiol* 93: 705–713, 2002.
11. **Bates JHT, Irvin CG.** Time dependence of recruitment and derecruitment in the lung: a theoretical model. *J Appl Physiol* 93: 705–713, 2002.
12. **Crotti S, Mascheroni D, Caironi P, Pelosi P, Ronzoni G, Mondino M, Marini JJ, Gattinoni L.** Recruitment and derecruitment during acute respiratory failure: a clinical study. *Am J Respir Crit Care Med* 164: 131–140, 2001.
13. **Dellinger RP, Levy MM, Carlet JM, Bion J, Parker MM, Jaeschke R, Reinhart K, Angus DC, Brun-Buisson C, Beale R, Calandra T, Dhainaut JF, Gerlach H, Harvey M, Marini JJ, Marshall J, Ranieri M, Ramsay G, Sevransky J, Thompson BT, Townsend S, Vender JS, Zimmerman JL, Vincent JL; International Surviving Sepsis Campaign Guidelines Committee; American Association of Critical-Care Nurses; American College of Chest Physicians; American College of Emergency Physicians; Canadian Critical Care Society; European Society of Clinical Microbiology and Infectious Diseases; European Society of Intensive Care Medicine; European Respiratory Society; International Sepsis Forum; Japanese Association for Acute Medicine; Japanese Society of Intensive Care Medicine; Society of Critical Care Medicine; Society of Hospital Medicine; Surgical Infection Society; World Federation of Societies of Intensive and Critical Care Medicine.** Surviving Sepsis Campaign: international guidelines for management of severe sepsis and septic shock: 2008. *Crit Care Med* 296–327. [Erratum. *Crit Care Med* 36 (Apr): 1394–1396, 2008.]
14. **Falke KJ, Pontoppidan H, Kumar A, Leith DE, Geffin B, Laver MB.** Ventilation with end-expiratory pressure in acute lung disease. *J Clin Invest* 51: 2315–2323, 1972.
15. **Ferguson ND, Cook DJ, Guyatt GH, Mehta S, Hand L, Austin P, Zhou Q, Matte A, Walter SD, Lamontagne F, Granton JT, Arabi YM, Arroliga AC, Stewart TE, Slutsky AS, Meade MO; OSCILLATE Trial Investigators; Canadian Critical Care Trials Group.** High-frequency oscillation in early acute respiratory distress syndrome. *N Engl J Med* 368: 795–805, 2013.
16. **Frawley PM, Habashi NM.** Airway pressure release ventilation and pediatrics: theory and practice. *Crit Care Nurs Clin North Am* 16: 337–348, viii, 2004.
17. **Gattinoni L, Caironi P.** Refining ventilatory treatment for acute lung injury and acute respiratory distress syndrome. *JAMA* 299: 691–693, 2008.
18. **Gattinoni L, Carlesso E, Valenza F, Chiumello D, Caspani ML.** Acute respiratory distress syndrome, the critical care paradigm: what we learned and what we forgot. *Curr Opin Crit Care* 10: 272–278, 2004.
19. **Gaver DP 3rd, Samsel RW, Solway J.** Effects of surface tension and viscosity on airway reopening. *J Appl Physiol* 69: 74–85, 1990.
20. **Grasso S, Terragni P, Birocco A, Urbino R, Del Sorbo L, Filippini C, Mascia L, Pesenti A, Zangrillo A, Gattinoni L, Ranieri VM.** ECMO criteria for influenza A (H1N1)-associated ARDS: role of transpulmonary pressure. *Intensive Care Med* 38: 395–403, 2012.
21. **Habashi NM.** Other approaches to open-lung ventilation: airway pressure release ventilation. *Crit Care Med* 33: S228–S240, 2005.
22. **Hantos Z, Daroczy B, Suki B, Nagy S, Fredberg JJ.** Input impedance and peripheral inhomogeneity of dog lungs. *J Appl Physiol* 72: 168–178, 1992.
23. **Harris RS.** Pressure-volume curves of the respiratory system. *Respir Care* 50: 78–98; discussion 98–79, 2005.
24. **Hough PD, Kolda TG, Torczon VJ.** Asynchronous parallel pattern search for nonlinear optimization. *SIAM J Sci Comput* 23: 134–156, 2001.
25. **Kolda TG.** Revisiting asynchronous parallel pattern search for nonlinear optimization. *SIAM J Optim* 16: 563–586, 2005.
26. **Kolda TG, Torczon VJ.** On the convergence of asynchronous parallel pattern search. *SIAM J Optim* 14: 939–964, 2004.
27. **Kollisch-Singule M, Emr B, Smith B, Roy S, Jain S, Satalin J, Snyder K, Andrews P, Habashi N, Bates JH, Marx W, Nieman G, Gatto L.** Mechanical breath profile of airway pressure release ventilation: the effect on alveolar recruitment and microstrain in acute lung injury. *JAMA Surg* 149: 1138–1145, 2014.
28. **Kollisch-Singule M, Emr B, Smith BJ, Ruiz C, Roy S, Meng Q, Jain S, Satalin J, Snyder K, Ghosh A, Marx W, Andrews P, Habashi N, Nieman G, Gatto L.** Airway pressure release ventilation reduces conducting airway micro-strain in lung injury. *J Am Coll Surg* 219: 968–976, 2014.
29. **Lewis RM, Torczon V.** Pattern search algorithms for bound constrained minimization. *SIAM J Optim* 9: 1082–1099, 1999.
30. **Ma B, Bates JHT.** Modeling the complex dynamics of derecruitment in the lung. *Ann Biomed Eng* 38: 3466–3477, 2010.
31. **Massa CB, Allen GB, Bates JHT.** Modeling the dynamics of recruitment and derecruitment in mice with acute lung injury. *J Appl Physiol* 105: 1813–1821, 2008.
32. **Matamis D, Lemaire F, Harf A, Brun-Buisson C, Ansquer JC, Atlan G.** Total respiratory pressure-volume curves in the adult respiratory distress syndrome. *Chest* 86: 58–66, 1984.
33. **Meade MO, Cook DJ, Guyatt GH, Slutsky AS, Arabi YM, Cooper DJ, Davies AR, Hand LE, Zhou Q, Thabane L, Austin P, Lapinsky S, Baxter A, Russell J, Skrobik Y, Ronco JJ, Stewart TE; Lung Open Ventilation Study Investigators.** Ventilation strategy using low tidal volumes, recruitment maneuvers, and high positive end-expiratory pressure for acute lung injury and acute respiratory distress syndrome: a randomized controlled trial. *JAMA* 299: 637–645, 2008.
34. **Medoff BD, Harris RS, Kesselman H, Venegas J, Amato MBP, Hess D.** Use of recruitment maneuvers and high positive end-expiratory pressure in a patient with acute respiratory distress syndrome. *Crit Care Med* 28: 1210–1216, 2000.
35. **Mercat A, Richard JC, Vielle B, Jaber S, Osman D, Diehl JL, Lefrant JY, Prat G, Richecoeur J, Nieszkowska A, Gervais C, Baudot J, Bouadma L, Brochard L; Expiratory Pressure (Express) Study Group.** Positive end-expiratory pressure setting in adults with acute lung injury and acute respiratory distress syndrome: a randomized controlled trial. *JAMA* 299: 646–655, 2008.
36. **Neumann P, Wrigge H, Zinserling A, Hinz J, Maripuu E, Andersson LG, Putensen C, Hedenstierna G.** Spontaneous breathing affects the spatial ventilation and perfusion distribution during mechanical ventilatory support. *Crit Care Med* 33: 1090–1095, 2005.
37. **Otis DR Jr, Johnson M, Pedley TJ, Kamm RD.** Role of pulmonary surfactant in airway closure: a computational study. *J Appl Physiol* 75: 1323–1333, 1993.
38. **Pelosi P, Goldner M, McKibben A, Adams A, Eccher G, Caironi P, Losappio S, Gattinoni L, Marini JJ.** Recruitment and derecruitment

during acute respiratory failure: an experimental study. *Am J Respir Crit Care Med* 164: 122–130, 2001.
39. **Rohrer F.** Der Strömungswiderstand in den menschlichen Atemwegen. *Pflugers Arch* 162: 225–259, 1915.
40. **Roy S, Habashi N, Sadowitz B, Andrews P, Ge L, Wang G, Roy P, Ghosh A, Kuhn M, Satalin J, Gatto LA, Lin X, Dean DA, Vodovotz Y, Nieman G.** Early airway pressure release ventilation prevents ARDS–a novel preventive approach to lung injury. *Shock* 39: 28–38, 2013.
41. **Roy S, Sadowitz B, Andrews P, Gatto LA, Marx W, Ge L, Wang G, Lin X, Dean DA, Kuhn M, Ghosh A, Satalin J, Snyder K, Vodovotz Y, Nieman G, Habashi N.** Early stabilizing alveolar ventilation prevents acute respiratory distress syndrome: a novel timing-based ventilatory intervention to avert lung injury. *J Trauma Acute Care Surg* 73: 391–400, 2012.
42. **Santa Cruz R, Rojas JI, Nervi R, Heredia R, Ciapponi A.** High versus low positive end-expiratory pressure (PEEP) levels for mechanically ventilated adult patients with acute lung injury and acute respiratory distress syndrome. *Cochrane Database Syst Rev* 6: CD009098, 2013.
43. **Schuessler TF, Bates JH.** A computer-controlled research ventilator for small animals: design and evaluation. *IEEE Trans Biomed Eng* 42: 860–866, 1995.
44. **Seah AS, Grant KA, Aliyeva M, Allen GB, Bates JHT.** Quantifying the roles of tidal volume and PEEP in the pathogenesis of ventilator-induced lung injury. *Ann Biomed Eng* 39: 1505–1516, 2011.
45. **Shari G, Kojicic M, Li G, Cartin-Ceba R, Alvarez CT, Kashyap R, Dong Y, Poulose JT, Herasevich V, Garza JA, Gajic O.** Timing of the onset of acute respiratory distress syndrome: a population-based study. *Respir Care* 56: 576–582, 2011.
46. **Smith BJ, Bates JH.** Variable ventilation as a diagnostic tool for the injured lung. *IEEE Trans Biomed Eng*. In press.
47. **Smith BJ, Grant KA, Bates JH.** Linking the development of ventilator-induced lung injury to mechanical function in the lung. *Ann Biomed Eng* 41: 527–536, 2013.
48. **Suter PM, Fairley B, Isenberg MD.** Optimum end-expiratory airway pressure in patients with acute pulmonary failure. *N Engl J Med* 292: 284–289, 1975.
49. **Villar J, Blanco J, Anon JM, Santos-Bouza A, Blanch L, Ambros A, Gandia F, Carriedo D, Mosteiro F, Basaldua S, Fernandez RL, Kacmarek RM.** The ALIEN study: incidence and outcome of acute respiratory distress syndrome in the era of lung protective ventilation. *Intensive Care Med* 37: 1932–1941, 2011.
50. **White DNJ.** Parallel pattern search energy minimization. *J Mol Graph* 15: 154–157, 1997.
51. **Wrigge H, Zinserling J, Neumann P, Defosse J, Magnusson A, Putensen C, Hedenstierna G.** Spontaneous breathing improves lung aeration in oleic acid-induced lung injury. *Anesthesiology* 99: 376–384, 2003.
52. **Wrigge H, Zinserling J, Neumann P, Muders T, Magnusson A, Putensen C, Hedenstierna G.** Spontaneous breathing with airway pressure release ventilation favors ventilation in dependent lung regions and counters cyclic alveolar collapse in oleic-acid-induced lung injury: a randomized controlled computed tomography trial. *Crit Care* 9: R780–R789, 2005.
53. **Wright JL, Sun JP, Vedal S.** A longitudinal analysis of pulmonary function in rats during a 12 month cigarette smoke exposure. *Eur Respir J* 10: 1115–1119, 1997.
54. **Young D, Lamb SE, Shah S, MacKenzie I, Tunnicliffe W, Lall R, Rowan K, Cuthbertson BH; OSCAR Study Group.** High-frequency oscillation for acute respiratory distress syndrome. *N Engl J Med* 368: 806–813, 2013.